Journal of Molecular Catalysis A: Chemical 395 (2014) 58–65

Contents lists available at ScienceDirect

Journal of Molecular Catalysis A: Chemical

journal homepage: www.elsevier.com/locate/molcata

Fibrous nano-silica containing immobilized Ni@Au core–shell nanoparticles: A highly active and reusable catalyst for the reduction of 4-nitrophenol and 2-nitroaniline

Xuanduong Le, Zhengping Dong*, Wei Zhang, Xinlin Li, Jiantai Ma*

College of Chemistry and Chemical Engineering, Gansu Provincial Engineering Laboratory for Chemical Catalysis, Lanzhou University, Lanzhou 730000, PR China

ARTICLE INFO

Article history:
Received 17 April 2014
Received in revised form 29 July 2014
Accepted 3 August 2014
Available online 10 August 2014

Keywords:
Fibrous nano-silica
Ni@Au core–shell nanoparticles
Reduction
4-Nitrophenol
2-Nitroaniline

ABSTRACT

A novel, dandelion-like fibrous nano-silica catalyst (Ni@Au/KCC-1) has been synthesized by modifying fibrous nano-silica (KCC-1) with Ni@Au core–shell nanoparticles (NPs). KCC-1 was prepared using a hydrothermal method and has a dandelion-like shape, high surface area, and easy accessibility; KCC-1 can also be functionalized with 3-mercaptopropyltriethoxysilane. The mercaptopropyl groups on the fibers act as robust anchors for the immobilization of Ni@Au NPs, thus preventing the aggregation of the Ni@Au NPs. We investigated the catalytic performance of the Ni@Au/KCC-1 nanocatalyst by reducing 4-nitrophenol to 4-aminophenol in the presence of $NaBH_4$ as a probe reaction. The resulting Ni@Au/KCC-1 nanocatalyst exhibited superior catalytic activity to Ni@Au NPs, which may be attributed to the high accessibility of the KCC-1 support material. To some extent, it also may be due to the poor aggregation of Ni@Au NPs on the KCC-1 nano-silica support. The Ni@Au/KCC-1 nanocatalyst also showed high catalytic activity when used to reduce 2-nitroaniline. It is noteworthy that using Ni cores to fabricate the active sites Ni@Au NPs resulted in a lower amount of Au needed than is typical, because most of the Au-NPs catalyzed reactions occur on the surfaces of the NPs. In addition, the Ni cores give the Ni@Au/KCC-1 nanocatalyst superparamagnetic properties that increase its ease of recovery by a powerful magnet, allowing for it to be reused. The abovementioned approach based on fibrous KCC-1 and Ni@Au NPs provided a useful platform for the fabrication of noble-metal-based nanocatalysts with easy accessibility and a low cost, which may allow for an efficient green alternative for various catalytic reductions.

1. Introduction

The use of noble metal nanoparticles (NPs) in catalysis has long been a topic of research because of their strong catalytic activities [1–5]. Among the reported noble metal NPs used in catalysis, gold NPs (AuNPs) are the most stable metal NPs, and have been extensively studied because of their size-related properties, which can be leveraged in various applications [6–10]. AuNPs are also widely recognized as one of the most promising catalysts for a number of reactions, including the reduction of nitrophenol [11–13], the hydrodechlorination of 2,4-dichlorophenol [14], the oxidation of CO [15,16], the aerobic selective oxidation of glucose to gluconate [17], and the C–C cross coupling reactions [18]. Because smaller AuNPs have a higher surface-to-volume ratio, the high catalytic activity of AuNPs in these reactions strongly depends on the active atoms at the NPs surface. As the particle sizes decrease, the surface energies of the AuNPs increase, making them unstable, and resulting in a high tendency for inter-particle aggregation [19]. This can reduce the catalytic efficiency of the catalysts. To overcome this disadvantage, AuNPs are often immobilized onto solid supports with mespores, including SBA-15 [20–22], Al_2O_3 [23–25], MCM-41 [26,27], and SBA-16 [28]. When using one of these Au-supported catalysts, the small AuNPs become dispersed mainly on the large, internal surfaces and pores of the support. A consequence of this is that the active sites inside the pores are not readily available, which limits their applications. Because of this, catalyst supports with good accessibility and high surface areas (that is, not inside the pores), are highly desirable.

On the other hand, for many reported noble metal NPs catalysts, catalytic steps take place always at the surface of the NPs. Because of this, the inner noble metal atoms of the NPs can be replaced by other non-noble metals such as Fe, Co and Ni in order to reduce

* Corresponding authors. Tel.: +86 931 8912577; fax: +86 931 8912582.
E-mail addresses: dongzhp@lzu.edu.cn (Z. Dong), majiantai@lzu.edu.cn (J. Ma).

http://dx.doi.org/10.1016/j.molcata.2014.08.002
1381-1169/

the use of the noble metal without sacrificing the overall performance of the catalyst [29]. In addition, the presence of Fe, Co and Ni in hybrid, core–shell NPs possess excellent stability, solvent compatibility, catalytic activity, and magnetic separability. All of these properties greatly enhance the potential application of these catalysts. Despite these advantages, to date, noble metal NPs catalysts that possess inactive cores, excellent catalytic activities, low-cost, and efficient recoverable properties are very rare.

Fibrous Nano-Silica (KCC-1) with high surface area and high accessibility was first reported in the year 2010 [30]. The unique properties of KCC-1 are useful for designing silica-supported catalysts, and the accessibility of their active sites can also easily be increased. In our previous work, we synthesized Ag/KCC-1 nanocatalyst which exhibited excellent catalytic activity for the reduction of 4-nitrophenol (4-NP) and 2-nitroaniline (2-NA) using sodium borohydride ($NaBH_4$) in water at room temperature owing to the easy accessibility of the active sites [31].

Here, we report the preparation of a novel nanocatalyst based on core–shell Ni@Au NPs modified dandelion-like fibrous nano-silica (Ni@Au/KCC-1). Using non-noble metal like Fe, Co, or Ni is ideal choices for the material used in the core of the noble metal NPs as all of them make the catalyst easy to recycle and reuse owing to their superparamagnetic properties. We characterized the catalytic activities of Ni@Au/KCC-1 in a model reaction (the reduction of 4-NP). The Ni@Au/KCC-1 showed high catalytic activities during the reduction of 4-NP as compared with not only Ni@Au NPs, but also other Au catalysts reported recently by other researchers. The Ni@Au/KCC-1 nanocatalyst also showed high catalytic activity during the reduction of 2-NA. The robust activity of this catalyst is attributed to its high accessibility and low likelihood of the aggregation of the Ni@Au NPs on the KCC-1 nano-silica support system. The replacement of Ni@Au NP cores by Ni atoms could reduce the use of Au without sacrificing the overall performance of the catalyst, and may also increase the ease of recovery and resuse of the catalyst. Thus, Ni@Au NPs immobilized on KCC-1 exhibited highly effective catalytic property, showing promising potential for the catalytic reduction of nitroaromatic compounds leading to their safe and eco-friendly disposal.

2. Experimental

2.1. Materials

Tetraethyl orthosilicate (TEOS), Nickel(II) acetylacetonate ($Ni(acac)_2$), Chloroauric acid ($HAuCl_4$), tiphenylphosphine (TPP), oleyl amine (OAm), 4-NP, 2-NA, and 3-mercaptopropyltriethoxysilane (MPTES) were purchased from Sigma Aldrich. Cyclohexane, pentanol, Cetylpyridinium bromide (CPB), and $NaBH_4$ were reagent-grade-quality and were purchased from Tianjing Guangfu Chemical Company (Tianjin, China). All reagents and solvents used for synthesis and measuring were used as supplied, with no modification.

2.2. Preparation of KCC-1

KCC-1 was prepared using the microwave-assisted hydrothermal technique, as previously reported in literature [30]. We also successfully synthesized KCC-1 using a hydrothermal method without microwave-assistance. Firstly, TEOS (2.5 g, 0.12×10^{-1} mol) was dissolved in a solution of cyclohexane (30 mL) and pentanol (1.5 mL). A stirred solution of CPB (1 g, 0.26×10^{-2} mol) and urea (0.6 g, 0.01 mol) in water (30 mL) was then added. Secondly, the above mixture was stirred for 30 min at room temperature, and the resulting solution was placed in a teflon-sealed hydrothermal reactor. The reaction mixture was heated at 120 °C for 5 h. After completion of the reaction, the mixture was allowed to cool to room temperature and the silica formed was isolated by centrifugation, washed with distilled water and acetone, and vacuum drying overnight. The as-synthesized material was then calcined at 550 °C for 6 h in air, obtained KCC-1.

2.3. Fabrication of the Ni@Au/KCC-1 nanocatalyst

The Ni@Au core–shell NPs were prepared following the work reported by Peng et al. [32]. The Ni@Au core–shell NPs were prepared method as follow. The first step is to obtain Au precursor which is crucial for the preparation of Ni@Au nanoparticles. In a typical synthesis, 1.364 g of TPP and 1 g of $HAuCl_4{\cdot}4H_2O$ were dissolved in 50 and 35 mL of ethanol, respectively, and then the obtained solutions were mixed together with slight agitation. White precipitates ($[(C_6H_5)_3P]AuCl$ complex) were generated from this process and were filtered and further washed several times with ethanol and acetone and dried in vacuum.

In the next step, 0.5 mmol of $Ni(acac)_2$ was added in 7 mL of oleylamine and then heated at 45 °C. To aid the formation of Ni nanoparticles, a small amount of $HAuCl_4{\cdot}4H_2O$ (5.00 mg) that was mixed with 0.2 mL of toluene was also added in the above solution. This reaction generated Au-seeded Ni nanoparticles that served as the core component of Ni@Au nanoparticles. The resulted solution was heated to 195 °C for 30 min. After that, the obtained solution was cooled to 155 °C and a solution containing 0.1 g of pre-made Au precursor in 1 mL of dichloromethane was quickly injected in the pre-prepared oleylamine solution containing Ni nanoparticles. After a short temperature drop (approximately to 120 °C) due to injection, the reaction temperature was kept at 140 °C for 30 min before the solution was cooled to room temperature. The synthesized products were washed and separated by repeated precipitation using the mixture of hexane and ethanol to obtain black powder which could be redispersed in hexane and dichloromethane for the purpose of further characterization.

The schematic describing the preparation of Ni@Au/KCC-1 is shown in Scheme 1.

KCC-1 nano-silica was functionalized with MPTES prior to the immobilization of Ni@Au NPs on its surface. KCC-1 (1 g) was added to 50 mL of anhydrous toluene under ultrasonic treatment for 10 min to disperse it homogeneously. Then, 0.3 g of MPTES was added dropwise, and the mixture was refluxed for 10 h in a N_2 atmosphere. The mixture was then cooled to room temperature and the resulting mercaptopropylfunctionalized KCC-1 (HS-KCC-1) was centrifuged; washed repeatedly with chloroform, dichloromethane, and ethanol; and finally dried in vacuum.

HS-KCC-1 (0.4 g) was ultrasonically dispersed in 50 mL H_2O, and 0.1 g of Ni@Au NPs was added. After being stirred and ultrasonically dispersed for 1 h, Ni@Au/KCC-1 was obtained by centrifugation and dried in a vacuum.

2.4. Catalytic reactions with Ni@Au NPs and Ni@Au/KCC-1 nanocatalyst

The reduction of 4-NP by $NaBH_4$ at room temperature was chosen as a model reaction for comparison of the catalytic performance of Ni@Au NPs and the Ni@Au/KCC-1 nanocatalyst. In short, 2.5 mL of aqueous 4-NP solution (0.12 mM, 3×10^{-7} mol) was mixed with 0.5 mL of freshly prepared aqueous $NaBH_4$ solution (0.5 M, 2.5×10^{-2} mol), resulting in the formation of a deep yellow solution. Then, 30.0 μL of catalyst (Ni@Au NPs; 2 mg/mL) was added to this resulting solution, and the reaction was allowed to proceed until the solution became colorless.

The catalytic reduction of 2-NA at room temperature was also chosen as a model reaction for investigating the catalytic activity of the Ni@Au/KCC-1 nanocatalyst. The procedure was

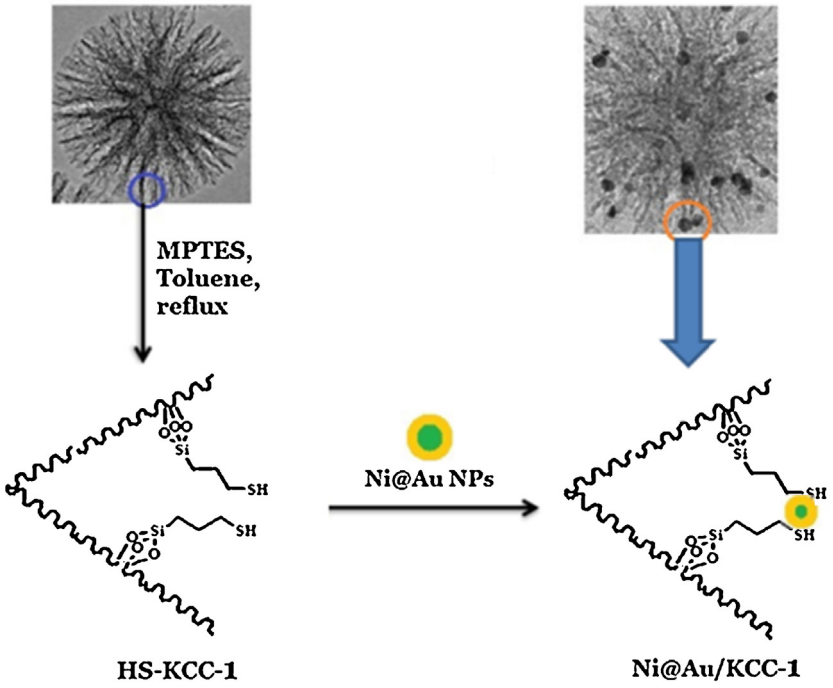

Scheme 1. Synthesis of Ni@Au/KCC-1 nanocatalyst.

as follows: 30 μL of catalyst (10 mg/mL, Ni@Au NPs 2 mg/mL) in an aqueous suspension (2.8 mL H_2O) was mixed with 40 μL of (1.26×10^{-2} mol/L, 5.04×10^{-7} mol) of 2-NA aqueous solution. Then, 0.13 mL (0.5 M, 0.65×10^{-4} mol) of $NaBH_4$ solution was injected rapidly while stirring. The color of the mixture vanished gradually; complete colorlessness indicated complete reduction. The progress of all reactions conducted here was monitored by measuring the UV–Vis absorption spectra of the reaction mixture.

2.5. The recovery and reuse of the Ni@Au/KCC-1 nanocatalyst

Reduction reactions were amplified 20× to characterize the reusability of the Ni@Au/KCC-1 nanocatalyst. The reaction conversion was determined by GC. The catalyst was recovered using a powerful magnet and then washed with water and ethanol and dried in a vacuum at room temperature before being used in the next catalytic run. The reduction of 4-NP and 2-NA catalytic process was carried out within 10 min for each cycle. This procedure was repeated ten times.

3. Results and discussion

3.1. Catalysts characterization

Ni@Au NPs were prepared as decomposition $[(C_6H_5)_3P]AuCl$ complexes on the surface of Ni NPs cores [32]. OAm was used as both the solvent and surfactant. Using $Ni(acac)_2$ as the starting material, the Ni core was first generated by adding Au seeds to the reaction mixture at 45 °C. Then, the $[(C_6H_5)_3P]AuCl$ complexes decomposed and the Au shell was formed at about 195 °C [32]. For the preparation of Ni@Au/KCC-1 nanocatalyst, the as-prepared KCC-1 nano-silica was functionalized with mercaptopropyl groups so that the Ni@Au NPs could be easily anchored onto the KCC-1 fibers (Scheme 1). The properties of KCC-1 and HS-KCC-1, including results of FTIR (Fig. S1), TGA (Fig. S2), Elemental analysis (Table S1) and surface areas (Table S1) are provided in the Supporting Information. The FTIR spectrum (Fig. S1) of HS-KCC-1 revealed the presence of mercaptopropyl groups, which provided binding sites for the adsorption of Ni@Au NPs onto the nano-silica surface. The results of TGA (Fig. S2) and the elemental analysis (Table S1) showed that the content of the MPTES grafted onto the surface of KCC-1 was about 0.2 mmol/g. The ICP-AES analysis we conducted showed that the proportion of the KCC-1 surface covered with Ni@Au NPs should be approximately 20%, which is similar to what we calculated in our experiment (Table S1).

Fig. 1a shows a TEM image of Ni@Au NPs. The diameter of the NPs is ranges from 8 to 18 nm, and the morphology of the NPs is near-spherical. The TEM image also reveals that a large number of Ni@Au NPs aggregated with each other. The selected area electron diffraction (SAED) pattern (Fig. 1a, *inset*) of these NPs exhibits mixed diffraction rings that belong to fcc-Au and fcc-Ni. In addition, the HRTEM image (Fig. 1b) verified the core–shell structure. The measured lattice fringes (0.238 nm) from the shell region correspond to Au (1 1 1) planes, whereas those measured from the core region (0.206 nm) are accordant to the Ni (1 1 1) planes, showing clear differences between the core and shell.

Fig. 1c (HAADF-STEM) revealed that Ni@Au nanoparticles have a brighter contrast at the edge and darker contrast in the core. Thus the core and shell have different chemical compositions was indicated. Because of Au have a much higher atomic number than Ni, it scatters electrons very intensively, therefore it was appeared bright in the HAADF image. The STEM-EDS (Fig. 1d) on a single particle clearly shown strong Au signals at the particle edge and strong Ni signals in the particle center revealed a typical core–shell structure.

KCC-1 has high accessibility, which has been attributed to its fibers [30,33]. Therefore, the unique properties of KCC-1 may be useful for the design of silica-supported catalysts, for which the accessibility of active sites can be increased significantly. The morphology of KCC-1 is shown in Fig. 1e. In the figure, KCC-1 microspheres with porous fibrous structure are uniform and monodisperse, with an average diameter of about 300 nm (Fig. 1e). The HRTEM image shown in Fig. 1e further clarifies that the distance between the two fibers is about 22 nm (Fig. 1e, *inset*). The large distance between fibers and the high surface area of KCC-1 (Table S1) make the Ni@Au NPs with diameters between 8 and 18 nm easily loaded onto KCC-1 nano-silica. It also prevents the aggregation of

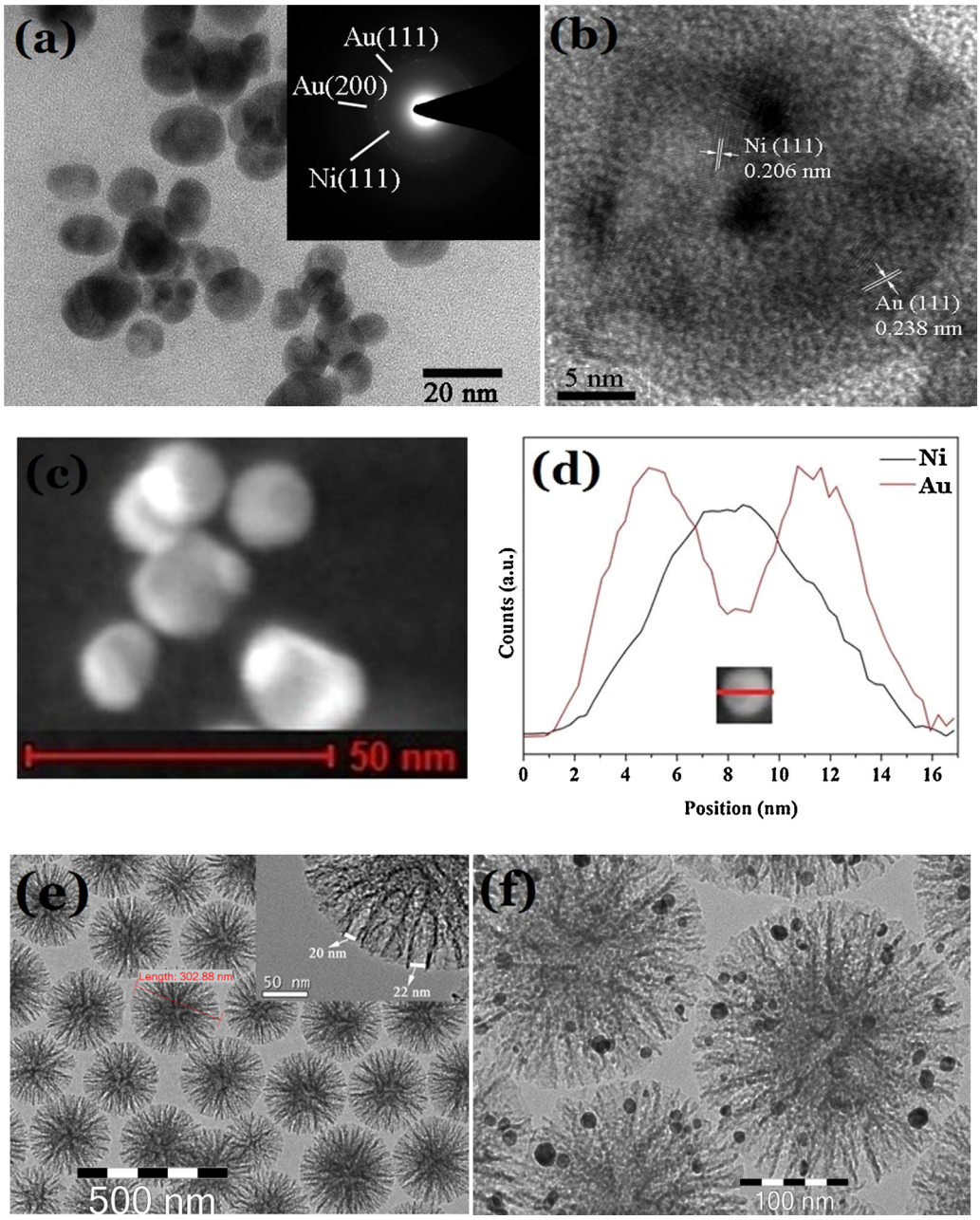

Fig. 1. (a) TEM image along with SAED pattern (inset) of Ni@Au NPs, (b) HRTEM image a single Ni@Au NP, (c) HAADF image showing the contrast between core (appear dark) and shell (appear bright) component, (d) STEM-EDS line-scan analysis of a single Ni@Au nanoparticle, (e) TEM images of KCC-1 with HRTEM image of KCC-1 (inset), (f) TEM image of Ni@Au/KCC-1.

the Ni@Au NPs and increases the accessibility of the active site of the nanocatalyst Ni@Au/KCC-1. A TEM image of the Ni@Au/KCC-1 sample is shown in Fig. 1f. The Ni@Au NPs are remarkably modified between the fibers of the KCC-1 microspheres, and no obvious aggregation is observed. When functionalized with MPTES, the mercaptopropyl groups may act as robust anchors for the immobilization of Ni@Au NPs. This process can also prevent the leaching of Ni@Au NPs from their support.

We used the EDS spectrum collected from energy dispersive X-ray analysis to determine the chemical composition of Ni@Au NPs. The peaks of Ni and Au are shown in Fig. 2a. This figure gives the Ni@Au NPs catalyst compositions (note that the Cu peak arises from the copper grid in TEM analysis). XRD analysis also can provide evidence for the composition of Ni@Au NPs. Fig. 2b reveals that Ni@Au NPs exhibit sharp peaks of Au (1 1 1), Ni (1 1 1), Au (2 0 0), Au (2 2 0) and Au (3 1 1) (JCPDS cards No. 04-0784), which also verify the exists of fcc-Au and fcc-Ni. The wide hump in the range of 2θ from 15° to 30° is typical for amorphous silica (for example, KCC-1). When the Ni@Au NPs were immobilized on the KCC-1 nano-silica surface, all of the characteristic, expected peaks of Ni@Au NPs were present, as was the amorphous silica peak. These results indicated that the immobilization of Ni@Au NPs was successful.

In order to examine the valence states of Au and Ni in the Ni@Au/KCC-1, XPS analysis was carried out (Fig. 2c). The XPS elemental survey scan of the surface of Ni@Au/KCC-1 microspheres revealed that silicon, oxygen, gold, nickel, and carbon are present in the samples. While the binding energy of the Ni 2p at 853 eV is much weaker than those of Au 4d and Au 4f, this is mainly attributed to the Ni atoms that were concentrated in the cores of Ni@Au NPs. As shown in Fig. 2c, the Au 4d binding energies at 353 and 335 eV,

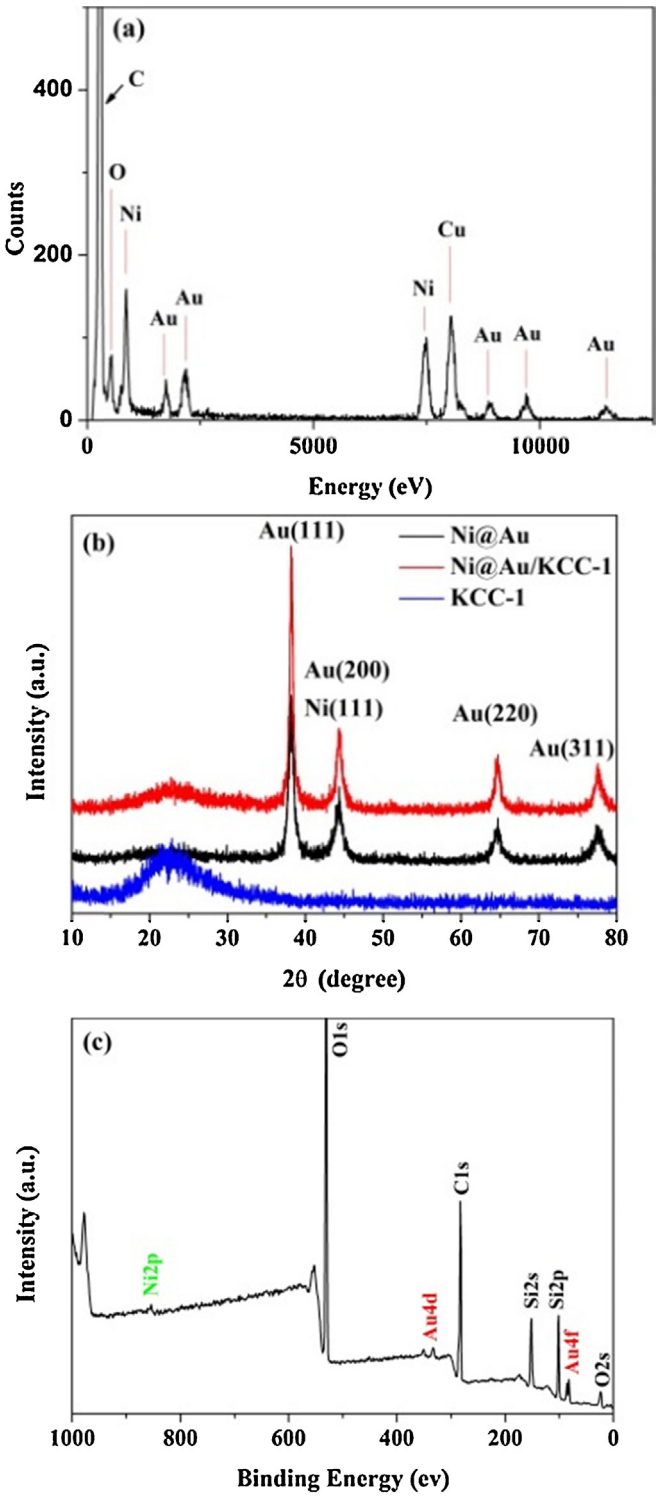

Fig. 2. (a) EDS spectra of Ni@Au NPs, (b) XRD pattern of KCC-1, Ni@Au NPs and Ni@Au/KCC-1, (c) XPS wide-scan spectrum of the Ni@Au/KCC-1.

and the Au 4f binding energies at 88 and 84 eV, are characteristic of metallic Au.

Magnetization curves (Fig. 3) show the superparamagnetic behavior of both the Ni@Au NPs and the Ni@Au/KCC-1 nanocatalyst. The magnetic saturation values of the Ni@Au NPs is 4.53 emu/g. When Ni@Au NPs were functionalized on the KCC-1, the magnetic saturation values were reduced to only 0.9 emu/g. However, the Ni@Au/KCC-1 nanocatalyst can still be easily separated from a

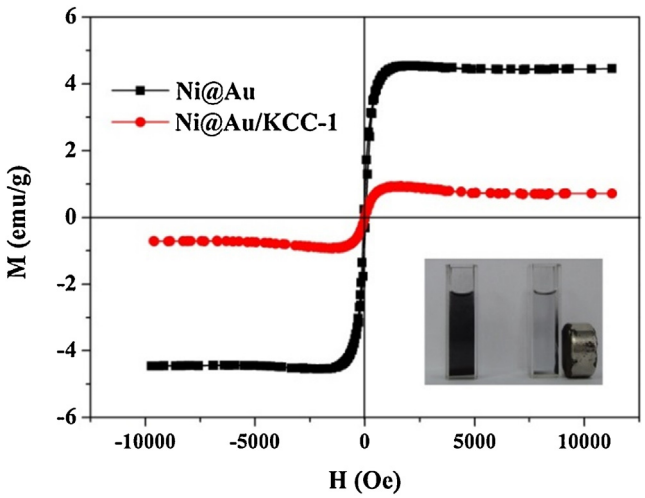

Fig. 3. Room temperature magnetization curves of Ni@Au NPs and Ni@Au/KCC-1.

reaction solution with the use of a powerful magnet (Fig. 3, *inset*), which makes the Ni@Au/KCC-1 nanocatalyst recoverable and able to be used repeatedly.

3.2. Catalytic tests

We investigated the catalytic performance of the Ni@Au/KCC-1 nanocatalyst by using the reduction of 4-NP into 4-AP in the presence of $NaBH_4$ as a probe reaction. The reaction was easily monitored by UV–Vis spectroscopy because the reactant (4-nitrophenolate anion) and product (4-AP) have different maximum absorption peaks, i.e., λ_{max} = 400 nm (reactant) and 300 nm (product) [34]. In comparison, Ni@Au NPs were also used for catalytic reducing the 4-NP.

Initially, the 4-NP solution has a light yellow color, which turns bright yellow upon the addition of $NaBH_4$. This colour change is due to the formation of 4-nitrophenolate (Fig. 4a, *inset*). This process is accompanied by a strong absorption peak of 317 nm for 4-NP, which is remarkably red-shifted to 400 nm following the reaction [35–37]. Even after adding superfluous $NaBH_4$, the maximum absorption of 400 nm did not change over time, which confirmed that the reduction did not proceed by aqueous $NaBH_4$ solution. The reduction of 4-NP $\left(E^0_{(4\text{-NP/4-AP})} = -0.76\,\text{V}\right)$ by $NaBH_4$ $\left(E^0_{(H_3BO_3/BH_4^-)} = -1.33\,\text{V}\right)$ is thermodynamically feasible but kinetically restricted in the absence of a catalyst [38].

When catalyst is introduced into the solution, the absorption at 400 nm decreases and absorption at 300 nm increases gradually, which indicates the replacement of 4-NP with 4-AP [39]. Visually, the color of the reaction mixture changes from yellow to colorless (Scheme 2), also indicating the replacement of 4-NP with 4-AP.

As shown in Fig. 4b, when 6×10^{-2} mg of Ni@Au catalyst was added to the reaction mixture, the reduction reaction completed in about 12 min, while for the Ni@Au/KCC-1 nanocatalyst with the same amount of Ni@Au NPs, the reduction reaction took only 10 min (Fig. 4c). This difference suggests that Ni@Au/KCC-1 has higher catalytic activity than Ni@Au NPs. This is likely due to the immobilization of the Ni@Au NPs onto the KCC-1 nano-silica, which overcomes the issue of aggregation and enhances the catalytic activity.

The concentration of $NaBH_4$ is much higher than that of 4-NP; thus, it can be considered essentially constant during the reaction. This high concentration also protects the 4-AP from aerial oxidation [40]. Therefore, we used pseudo first-order kinetics with respect to

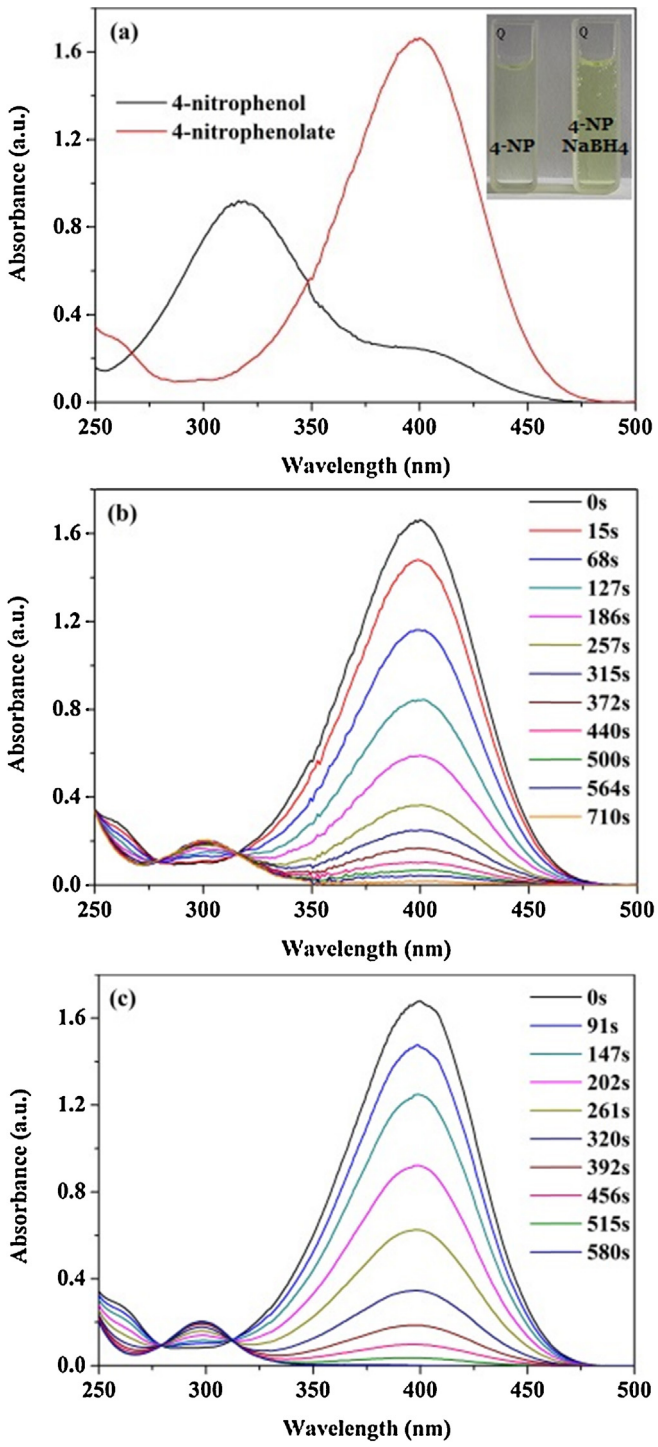

Fig. 4. UV–Vis spectra of 4-NP before and after adding NaBH4 solution (a), and the successive reduction of 4-NP to 4-AP over the prepared catalysts: (b) Ni@Au NPs and (c) Ni@Au/KCC-1.

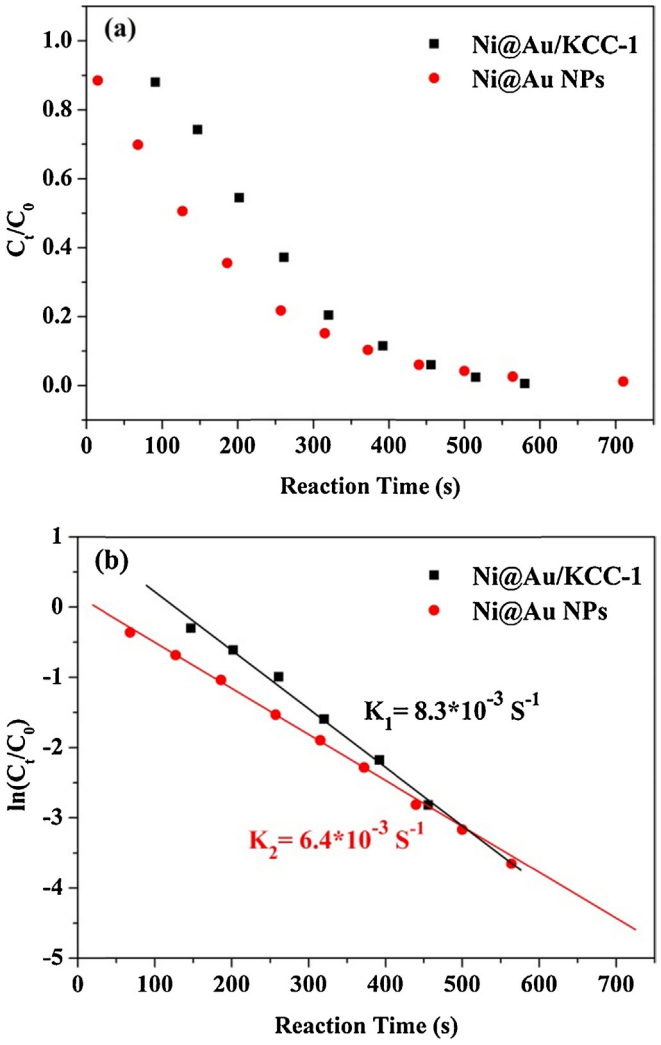

Fig. 5. Plots of C_t/C_0 (a) and $\ln(C_t/C_0)$ (b) versus reaction time for the reduction of 4-NP over Ni@Au NPs and Ni@Au/KCC-1.

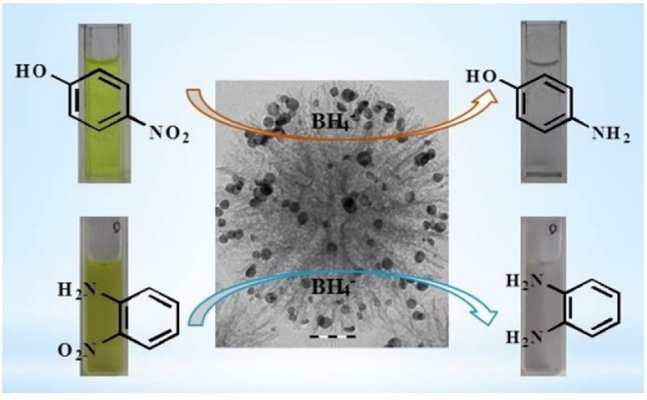

Scheme 2. The reduction of 4-NP and 2-NA on the surfaces of Ni@Au/KCC-1 catalyst.

4-NP to calculate the catalytic rate. The reaction conversion was calculated from C_t/C_0 (Fig. 5a), which was measured using the relative intensity of UV–Vis absorbance (A_t/A_0) at 400 nm. C_t is the concentration of 4-NP at reaction time t; C_0 is the initial concentration. As shown in Fig. 5b, the linear correlation between $\ln(C_t/C_0)$ and reaction time demonstrates that the 4-NP reduction reaction is of the first-order. Thus, the kinetic equation of this catalytic reaction is: $\ln(C_t/C_0) = -kt$, where k is the apparent first-order rate constant (s^{-1}), and t is the reaction time. We calculated the reaction rate constant k to be 6.4×10^{-3} and $8.3 \times 10^{-3}\ s^{-1}$ for the Ni@Au NPs and Ni@Au/KCC-1 catalyzed reductions of 4-NP, respectively.

For a quantitative comparison, the activity parameter $k' = k/M$ was introduced, which is the ratio of the rate constant k to the weight of the active sites Au added (M) [35,38]. Using this equation, the reaction rate constant per unit mass (M_{Au}) was calculated to be 307 and 237 $s^{-1}\ g^{-1}$ for the reduction of 4-NP using Ni@Au/KCC-1 and Ni@Au NPs, respectively. The Ni@Au/KCC-1 nanocatalyst

Table 1
The comparison of catalytic activities for the reduction of 4-NP with catalysts reported in literatures.

Catalyst	Catalyst used (mg)	Au content (%)	k (s^{-1})[a]	k/M_{Au} (s^{-1} g^{-1})[b]
Au/graphene [47]	0.1	24	3.17×10^{-3}	132
Carbon@Au [48]	0.1	22.7	5.42×10^{-3}	239
Ni@Au NPs (this work)	6×10^{-2}	45	6.4×10^{-3}	237
Ni@Au/KCC-1 (this work)	0.3	9	8.3×10^{-3}	307

[a] The reaction rate constant.
[b] The reaction rate constant per total weight of Au in the used catalyst.

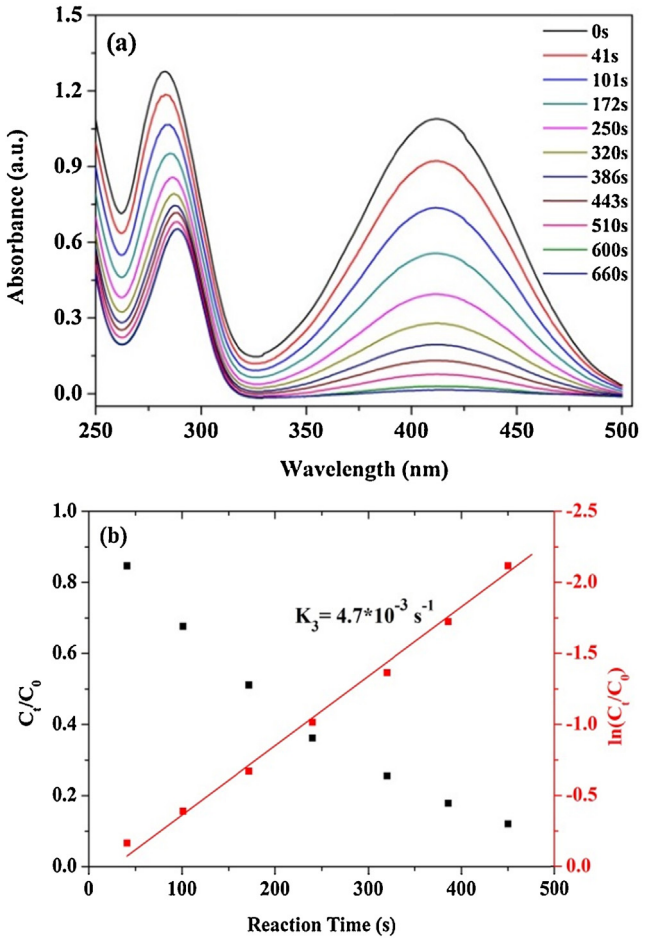

Fig. 6. (a) UV–Vis spectra the successive reduction of 2-NA to o-PDA over Ni@Au/KCC-1 catalyst, (b) Plots of C_t/C_0 and $\ln(C_t/C_0)$ versus reaction time for the reduction of 2-NA to o-PDA over Ni@Au/KCC-1 nanocatalyst.

clearly had higher catalytic activity than Ni@Au NPs. This was likely due to the ease of accessibility of the Ni@Au/KCC-1 nanocatalyst's active site, and the low amount of aggregation of Ni@Au NPs on the KCC-1 nano-silica support.

Based on our above results, we also used the Ni@Au/KCC-1 nanocatalyst to perform the catalytic reduction of 2-NA. The reduction of 2-NA can also be easily monitored because the product for the reduction reaction was only, the progress of the reaction can be determined by measuring the change in UV–Vis absorbance [9,37,41–46]. As shown in Fig. 6a, 2-NA shows a typical absorbance peak at 410 nm. When the Ni@Au/KCC-1 nanocatalyst was added, the absorbance peak intensity decreased gradually as 2-NA was reduced into *o*-PDA. As shown in Fig. 6b, the linear correlation between $\ln(C_t/C_0)$ and the reaction time (t) confirms that the 2-NA reduction reaction is a first-order reaction. The reaction rate constant calculated from the linear slope was 4.7×10^{-3} s^{-1}. The

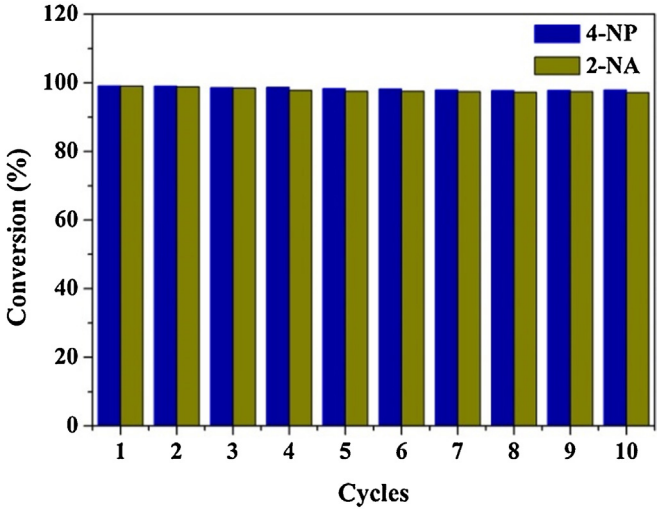

Fig. 7. The reusability of Ni@Au/KCC-1 nanocatalyst as a catalysts for the reduction of 4-NP and 2-NA with $NaBH_4$.

reaction rate constant per unit mass (M_{Au}) was calculated to be 174 s^{-1} g^{-1}.

The comparison of the catalytic activity of the Ni@Au/KCC-1 nanocatalyst with Ni@Au NPs and other reported Au NP-based catalysts in the reduction of 4-NP are listed in Table 1. Our results showed that the reaction rate constant per total weight of Au for Ni@Au/KCC-1 is higher than that of the unsupported Ni@Au NPs. It is also higher than the Au/graphene catalyst (132 s^{-1} g^{-1}) and the carbon@Au core–shell nanofiber catalyst (239 s^{-1} g^{-1}) reported previously [47,48]. The good catalytic activity of the Ni@Au/KCC-1 nanocatalyst owes to the ease of access of its active site, and the low aggregation of the Ni@Au NPs on the KCC-1 support. In this situation, both 4-NP and BH_4^- can be easily adsorbed on the Ni@Au NPs surface, which allows the reduction reactions to start quickly and finish rapidly.

One of the advantages of the Ni@Au/KCC-1 nanocatalyst that we present here is that the recovery of the catalyst is easily achieved by magnetic separation, because the Ni@Au NPs have magnetic cores. This allows the NPs to be reused for the next catalytic run. As shown in Fig. 7, the recovered Ni@Au/KCC-1 nanocatalyst exhibited almost constant catalytic activity for at least ten successive cycles in both the reduction of 4-NP and the reduction of 2-NA, with stable conversions above 97% within 10 min. This result suggests that the Ni@Au/KCC-1 nanocatalyst possesses robust stability.

4. Conclusion

In conclusion, we have successfully developed a novel, fibrous nano-silica catalyst called Ni@Au/KCC-1. This nanocatalyst, with Ni@Au NPs as the active sites, can not only reduce the use of Au without reducing catalytic activity, but can also confer superparamagnetic properties to the nanocatalyst, making the catalyst easy to recover for reuse. The Ni@Au/KCC-1 nanocatalyst exhibited

excellent catalytic activity in its reduction of 4-NP and 2-NA, which may be attributed to the high accessibility of the KCC-1 support material and the low amount of aggregation of the Ni@Au NPs on the KCC-1 support. Furthermore, Ni@Au/KCC-1 can be reused at least ten times without an obvious reduction in catalytic activity. This is partially due to the prevention of leaching of Ni@Au NPs from the mercaptopropyl groups' functionalized fibrous support. Our study offers a new strategy for the preparation of core–shell, noble metal, NP-based nanocatalysts with easy accessibility and high catalytic activity. This process may be used in the future to develop additional nanocatalysts that possess favorable properties, such as efficiency and ease of reuse.

Acknowledgements

The authors acknowledge financial support from the NSFC (Grants 21301082), the Natural Science Foundation of Gansu (No. 1308RJYA028) and the Fundamental Research Funds for the Central Universities (lzujbky-2013-61).

Appendix A. Supplementary data

Supplementary data associated with this article can be found, in the online version, at http://dx.doi.org/10.1016/j.molcata.2014.08.002.

References

[1] M.L. Wang, T.T. Jiang, Y. Lu, H.J. Liu, Y. Chen, J. Mater. Chem. A 1 (2013) 5923–5933.
[2] X. Zhang, Z. Su, Adv. Mater. 24 (2012) 4574–4577.
[3] Z.M. de Pedro, E. Diaz, A.F. Mohedano, J.A. Casas, J.J. Rodriguez, Appl. Catal. B: Environ. 103 (2011) 128–135.
[4] Y.M. Liu, H. Tsunoyama, T. Akita, S.H. Xie, T. Tsukuda, ACS Catal. 1 (2011) 2–6.
[5] X. Yang, C. Huang, Z.Y. Fu, H.Y. Song, S.J. Liao, Y.L. Su, L. Du, X.J. Li, Appl. Catal. B: Environ. 140 (2013) 419–425.
[6] Z.Y. Zhong, J.Y. Lin, S.P. Teh, J. Teo, F.M. Dautzenberg, Adv. Funct. Mater. 17 (2007) 1402–1408.
[7] F. Wang, X. Liu, C.-H. Lu, I. Willner, ACS Nano 7 (2013) 7278–7286.
[8] H. Miyamura, R. Matsubara, Y. Miyazaki, S. Kobayashi, Angew. Chem. Int. Ed. 46 (2007) 4151–4154.
[9] H. Gu, J. Wang, Y. Ji, Z. Wang, W. Chen, G. Xue, J. Mater. Chem. A 1 (2013) 12471–12477.
[10] X. Wang, H. Liu, D. Chen, X. Meng, T. Liu, C. Fu, N. Hao, Y. Zhang, X. Wu, J. Ren, F. Tang, ACS Appl. Mater. Inter. 5 (2013) 4966–4971.
[11] Y.C. Chang, D.H. Chen, J. Hazard. Mater. 165 (2009) 664–669.
[12] S.N. Wang, M.C. Zhang, W.Q. Zhang, ACS Catal. 1 (2011) 207–211.
[13] A. Gangula, R. Podila, M. Ramakrishna, L. Karanam, C. Janardhana, A.M. Rao, Langmuir 27 (2011) 15268–15274.
[14] S. Gomez-Quero, F. Cardenas-Lizana, M.A. Keane, J. Catal. 303 (2013) 41–49.
[15] X. Xu, Q. Fu, X. Guo, X. Bao, ACS Catal. 3 (2013) 1810–1818.
[16] X.T. Nie, H.F. Qian, Q.J. Ge, H.Y. Xu, R.C. Jin, ACS Nano 6 (2012) 6014–6022.
[17] I.V. Delidovich, B.L. Moroz, O.P. Taran, N.V. Gromov, P.A. Pyrjaev, I.P. Prosvirin, V.I. Bukhtiyarov, V.N. Parmon, Chem. Eng. J. 223 (2013) 921–931.
[18] M.G. Speziali, A.G.M. da Silva, D.M.V. de Miranda, A.L. Monteiro, P.A. Robles-Dutenhefner, Appl. Catal. A: Gen. 462 (2013) 39–45.
[19] Y. Lin, Y. Qiao, Y. Wang, Y. Yan, J. Huang, J. Mater. Chem. 22 (2012) 18314–18320.
[20] N. Anand, P. Ramudu, K.H.P. Reddy, K.S.R. Rao, B. Jagadeesh, V.S.P. Babu, D.R. Burri, Appl. Catal. A: Gen. 454 (2013) 119–126.
[21] X.Y. Liu, A.Q. Wang, X.D. Wang, C.Y. Mou, T. Zhang, Chem. Commun. 27 (2008) 3187–3189.
[22] L. Wang, H. Wang, P. Hapala, L.F. Zhu, L.M. Ren, X.J. Meng, J.P. Lewis, F.S. Xiao, J. Catal. 281 (2011) 30–39.
[23] L.X. Xu, C.H. He, M.Q. Zhu, S. Fang, Catal. Lett. 114 (2007) 202–205.
[24] R.H. Liu, N.S. Gao, F. Zhen, Y.Y. Zhang, L. Mei, X.W. Zeng, Chem. Eng. J. 225 (2013) 245–253.
[25] L. Storaro, M. Lenarda, E. Moretti, A. Talon, F. Porta, B. Moltrasio, P. Canton, J. Colloid Interface Sci. 350 (2010) 435–442.
[26] I. Sobczak, A. Kusior, J. Grams, M. Ziolek, J. Catal. 245 (2007) 259–266.
[27] P.R. Selvakannan, K. Mantri, J. Tardio, S.K. Bhargava, J. Colloid Interface Sci. 394 (2013) 475–484.
[28] Y.J. Hao, Y.Z. Chong, S.R. Li, H.Q. Yang, J. Phys. Chem. C 116 (2012) 6512–6519.
[29] O. Metin, S.F. Ho, C. Alp, H. Can, M.N. Mankin, M.S. Gultekin, M. Chi, S. Sun, Nano Res. 6 (2013) 10–18.
[30] V. Polshettiwar, D. Cha, X. Zhang, J.M. Basset, Angew. Chem. Int. Ed. 49 (2010) 9652–9656.
[31] Z. Dong, X. Le, X. Li, W. Zhang, C. Dong, J. Ma, Appl. Catal. B: Environ. 158–159 (2014) 129–135.
[32] H. She, Y. Chen, X. Chen, K. Zhang, Z. Wang, D.-L. Peng, J. Mater. Chem. 22 (2012) 2757–2765.
[33] A. Fihri, D. Cha, M. Bouhrara, N. Almana, V. Polshettiwar, ChemSusChem 5 (2012) 85–89.
[34] H. Fu, X. Yang, X. Jiang, A. Yu, Langmuir 29 (2013) 7134–7142.
[35] J. Zhang, G. Chen, M. Chaker, F. Rosei, D. Ma, Appl. Catal. B: Environ. 132 (2013) 107–115.
[36] H. Yamamoto, H. Yano, H. Kouchi, Y. Obora, R. Arakawa, H. Kawasaki, Nanoscale 4 (2012) 4148–4154.
[37] B. Xia, F. He, L. Li, Langmuir 29 (2013) 4901–4907.
[38] B. Baruah, G.J. Gabriel, M.J. Akbashev, M.E. Booher, Langmuir 29 (2013) 4225–4234.
[39] G. Marcelo, A. Munoz-Bonilla, M. Fernandez-Garcia, J. Phys. Chem. C 116 (2012) 24717–24725.
[40] J. Huang, S. Vongehr, S. Tang, X. Meng, J. Phys. Chem. C 114 (2010) 15005–15010.
[41] J. Zheng, Y. Dong, W. Wang, Y. Ma, J. Hu, X. Chen, X. Chen, Nanoscale 5 (2013) 4894–4901.
[42] A. Shivhare, S.J. Ambrose, H. Zhang, R.W. Purves, R.W.J. Scott, Chem. Commun. 49 (2013) 276–278.
[43] K. Jiang, H.-X. Zhang, Y.-Y. Yang, R. Mothes, H. Lang, W.-B. Cai, Chem. Commun. 47 (2011) 11924–11926.
[44] F. Gonzalez de Rivera, I. Angurell, M.D. Rossell, R. Erni, J. Llorca, N.J. Divins, G. Muller, M. Seco, O. Rossell, Chem. Eur. J. 19 (2013) 11963–11974.
[45] X. Li, X. Wang, S. Song, D. Liu, H. Zhang, Chem. Eur. J. 18 (2012) 7601–7607.
[46] Y. Zhang, X. Yuan, Y. Wang, Y. Chen, J. Mater. Chem. 22 (2012) 7245–7251.
[47] J. Li, C.Y. Liu, Y. Liu, J. Mater. Chem. 22 (2012) 8426–8430.
[48] P. Zhang, C.L. Shao, X.H. Li, M.Y. Zhang, X. Zhang, C.Y. Su, N. Lu, K.X. Wang, Y.C. Liu, Phys. Chem. Chem. Phys. 15 (2013) 10453–10458.